Report No. UCB/SEMM-2013/06	Structural Engineering Mechanics and Materials
	Stability of Spinning Viscoelastic Cylinders at Finite Deformation By Sanjay Govindjee, Trevor Potter, and Jon Wilkening
July 2013	Department of Civil and Environmental Engineering University of California, Berkeley

Stability of spinning viscoelastic cylinders at finite deformation

Sanjay Govindjee[a,*], Trevor Potter[b], Jon Wilkening[b]

[a]*Department of Civil Engineering, University of California, Berkeley, Berkeley, CA 94720-1710, USA*
[b]*Department of Mathematics, University of California, Berkeley, Berkeley, CA 94720-3840, USA*

Abstract

The study of spinning axisymmetric cylinders undergoing finite deformation is a classic problem in several industrial settings – the tire industry in particular. The elastic formulation of the problem shows bifurcations into N-peak standing waves at rotational frequencies where the linearized evolution operator becomes singular. While standing-wave solutions are recognized to exist in the viscoelastic setting, there has been little study of their behavior. In this work we present a formulation of the problem that allows us to re-examine the elastic case and discover a second hierarchy of standing wave bifurcations. Additionally, with this framework we are able to study the viscoelastic case and show the existence of pseudo-bifurcation modes. This analysis also permits us to study the validity of two popular models for finite viscoelasticity. We show that the commonly used linear convolution model results in a non-physical exponential energy growth when the system is perturbed in a pseudo-bifurcation direction and followed in time. On the other hand, Sidoroff-style viscoelastic models are seen to be fully stable on pseudo-bifurcation branches as is physically required.

Keywords: rolling, tires, bifurcation, standing wave, viscoelasticity

*Corresponding author. Tel.: +1-510-642-6060
Email addresses: `s_g@berkeley.edu` (Sanjay Govindjee), `potter@math.berkeley.edu` (Trevor Potter), `wilkening@berkeley.edu` (Jon Wilkening)

1. Introduction

The behavior of steady spinning bodies at finite deformation is of both theoretical and practical interest. In the special case that the body is axisymmetric, there has been a fair amount of work devoted to its formulation, elucidation, and behavior. Notable early work on the spinning axisymmetric body was due to Padovan and Paramodilok [20, 21], Oden and Lin [18], Padovan [19], Bass [2], and Kennedy and Padovan [13]. This literature formulates the equations of motion in the frame of reference of a non-spinning observer translating alongside the rotating body, and then to various degrees examines the equilibrium solutions of the motion as the spin rate is varied. The issues of contact with "roadways" and viscoelastic as well as elastic response are considered. The work of LeTallec and Rahier [15], which followed this early work, provided the first clear description of the problem's kinematics and, by virtue thereof, laid the groundwork for the proper understanding of the issues associated with correctly specifying the constitutive response of a spinning body in a non-spinning frame of reference; see Govindjee and Mihalic [11] for a discussion of this point, and the work of Faria et al. [10], which shows that the issue was somewhat understood prior to these latter two works.

A special feature of the response of a steady spinning elastic body is the existence of non-axisymmetric solutions (standing waves) that appear as bifurcations from an axisymmetric branch in the configuration space of the body [18, 4]. The determination of these bifurcation speeds can be performed by searching for the spin rates at which the tangent operator of the equations of motion becomes singular. The bifurcated state can be determined by examining the eigenvector corresponding to the zero eigenvalue. Similar non-axisymmetric steady spinning solutions have also been reported upon in the case of finite deformation viscoelasticity [20, 21, 13, 4]. In the viscoelastic case one does not strictly find bifurcations such as are present in the elastic setting; rather, one finds analogous solutions with a similar spatial structure. Even though these solutions are "known" to exist, they have not been studied in detail beyond the linear setting of Chatterjee et. al [4]. This is a major goal of what follows.

An important issue when considering the mechanical response of continuum bodies is that the constitutive relations that are selected must satisfy the Clausius-Duhem inequality for satisfaction of the second law of thermodynamics; see e.g. Coleman and Noll [8] or Truesdell and Noll [27, §79]. In

the finite deformation viscoelastic setting there are two approaches to setting up the needed constitutive relations such that they will satisfy this condition. One, due to Coleman [7, 6], is to construct a free energy functional of the history of the material whose derivative with respect to the current measure of deformation yields a history functional giving the stress response. This framework seems natural for convolution type viscoelastic models, such as the well-known BKZ model [3] and the Simo model [26]. Notwithstanding the popular status of these two models, and the formal appearance of convolution expressions in their specification, the requisite free-energy functional that generates them has never been reported. In other words, while these models have the appearance of being strictly dissipative, it is actually not known if they satisfy the Clausius-Duhem inequality – this is in contrast to their behavior in the infinitesimal strain limit where they are known to satisfy the second law of thermodynamics. An alternate viscoelastic framework is provided by the work of Sidoroff [25], who proposes a multiplicative split of the deformation gradient, similar to finite deformation plasticity models, and then directly constructs evolution laws for the viscoelastic variables that satisfy the Clausius-Duhem inequality. Well known examples of models of this type are due to LeTallec and Rahier [15] and Reese and Govindjee [24]. The spinning body problem provides an ideal setting for a deep comparison of these two distinctly different modeling frameworks. In particular we will be able to demonstrate that the models of the Simo-class lead to non-physical results; whereas, the models of the Sidoroff-class behave well in similar situations. This point is particularly relevant for analysis schemes that rely upon a steady spinning state of a system followed by transient computation – e.g. in the modeling of a tire traveling at high speed that encounters a bump in the road.

An outline of the remainder of the paper is as follows: In §2 we review the strong and weak formulation of the elastic spinning body problem in both the steady and unsteady cases along with a discussion of its Hamiltonian structure. In §3 we revisit the well-studied elastic bifurcation case to show that our particular formulation is consistent with past work. We then go further to elucidate a second hierarchy of bifurcation solutions that have not been reported in numerical studies to our knowledge, but was mathematically foreshadowed in the monograph of Oden and Rabier [22]. With this background, in §4 we present two viscoelastic models in a form suitable for the study of spinning bodies. This is followed in §5 by an analysis of the behavior of spinning viscoelastic bodies and the strong influence of

the choice of viscoelastic modeling framework. In §6 we show that convolution type viscoelastic models can lead to non-physical instabilities at high rotation speeds that are not observed using either a purely elastic response or a Sidoroff-style viscoelastic model. The paper concludes with some brief comments and recommendations.

2. Elastic model

2.1. Domain and boundary conditions

The reference configuration $\mathcal{B}$ under consideration is an annulus centered at the origin with inner radius r_1 and outer radius r_2. Denoting material points $X = (X_1, X_2)$, we can write

$$\mathcal{B} = \{(X_1, X_2) \mid r_1 \leq \|X\|_2 \leq r_2\} \,. \tag{2.1}$$

We have inner boundary $\Gamma_h = \{X \mid \|X\|_2 = r_1\}$ called the hub and outer boundary $\Gamma_e = \{X \mid \|X\|_2 = r_2\}$ called the edge; see Fig. 1.

The hub is spun counter-clockwise about the origin at a constant angular velocity ω. If $\boldsymbol{\phi}$ is the motion of the body, then we have the boundary condition

$$\boldsymbol{\phi}(X, t) = \mathbf{R}(t)X \text{ on } \Gamma_h \,, \tag{2.2}$$

where $\mathbf{R}(t)$ is the rotation matrix given by

$$\mathbf{R}(t) = \begin{bmatrix} \cos(\omega t) & -\sin(\omega t) \\ \sin(\omega t) & \cos(\omega t) \end{bmatrix}. \tag{2.3}$$

On the edge, Γ_e, we prescribe traction-free boundary conditions.

2.2. Elastic constitutive equations

The motion is given by $\boldsymbol{\phi}(X, t)$ with deformation gradient $\mathbf{F} = D\boldsymbol{\phi} = \partial\boldsymbol{\phi}/\partial X$. We assume a plane strain elastic response described by a compressible Mooney-Rivlin model, with stored energy function $\boldsymbol{\Psi}_e(I_1, I_2, I_3)$. $\boldsymbol{\Psi}_e$ is given in terms of the invariants of the three dimensional right Cauchy-Green tensor

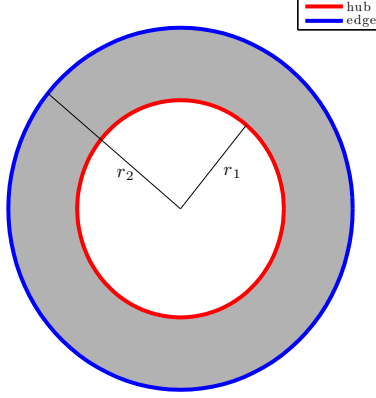$$\mathbf{C}_3 = \begin{bmatrix} \mathbf{C} & 0 \\ 0 & 1 \end{bmatrix}, \tag{2.4}$$

Figure 1: The reference domain $\mathcal{B}$.

where $\mathbf{C} = \mathbf{F}^{\mathsf{T}}\mathbf{F}$. We choose the stored energy function

$$\mathbf{\Psi}_e = \frac{\kappa}{4}\left(I_3 - \log I_3 - 1\right) + \frac{\mu}{2}(1-s)\left(I_1 - \log I_3 - 3\right) + \frac{\mu}{2}s\left(I_2 - 2\log I_3 - 3\right).$$

$$(2.5)$$

Here $\kappa > 0$ is the bulk modulus, $\mu > 0$ is the shear modulus, and $s \in [0,1]$ can be chosen to balance the two shear terms. This stored energy function is noted to be polyconvex [5, §4.9] and satisfy the conditions for Ball's theory [1] of existence of solutions in finite deformation elasticity. From this expression, we can compute the first Piola-Kirchhoff stress tensor $\mathbf{P}_e$:

$$\mathbf{P}_e = \frac{\partial \mathbf{\Psi}_e}{\partial \mathbf{F}} = \frac{\kappa}{2}(I_3-1)\mathbf{F}^{-T} + \mu(1-s)(\mathbf{F}-\mathbf{F}^{-T}) + \mu s(I_1\mathbf{F} - \mathbf{F}\mathbf{C} - 2\mathbf{F}^{-T}). \quad (2.6)$$

2.3. Equations of motion

Given $\mathbf{P}_e$, the elastic equations of motion are formulated as

$$\rho_R \ddot{\boldsymbol{\phi}} = \mathrm{DIV}\,\mathbf{P}_e \quad \text{on } \mathcal{B} \tag{2.7}$$

with boundary conditions

$$\begin{aligned} \boldsymbol{\phi}(X,t) &= \mathbf{R}(t)X \quad &\text{on } \Gamma_h \\ \mathbf{P}_e\mathbf{N} &= \mathbf{0} \quad &\text{on } \Gamma_e \,. \end{aligned} \tag{2.8}$$

ρ_R is the density of the undeformed material, which is assumed to be constant.

5

We reduce this second order equation in time to a system of first order equations in time by introducing the velocity of the motion, $\boldsymbol{\nu}(X,t)$, as an independent field variable. The equations of motion then become:

$$\dot{\boldsymbol{\phi}} = \boldsymbol{\nu} \qquad \text{on } \mathcal{B}$$
$$\dot{\boldsymbol{\nu}} = \frac{1}{\rho_R} \operatorname{DIV} \mathbf{P}_e \quad \text{on } \mathcal{B} \tag{2.9}$$

with boundary conditions

$$\boldsymbol{\phi}(X,t) = \mathbf{R}(t)X \quad \text{on } \Gamma_h$$
$$\boldsymbol{\nu}(X,t) = \dot{\mathbf{R}}(t)X \quad \text{on } \Gamma_h \tag{2.10}$$
$$\mathbf{P}_e \mathbf{N} = \mathbf{0} \qquad \text{on } \Gamma_e .$$

2.4. Steady spinning equations

We seek steady spinning states of the elastic body. Such a solution should satisfy

$$\boldsymbol{\phi}(X,t) = \boldsymbol{\phi}(\mathbf{R}(t)X,0)$$
$$\boldsymbol{\nu}(X,t) = \boldsymbol{\nu}(\mathbf{R}(t)X,0) \tag{2.11}$$

for all t. Following [15, 18, 11] among others, we introduce a new spatial variable $\widetilde{X}$ defined by

$$\widetilde{X} = \mathbf{R}(t)X. \tag{2.12}$$

We then define

$$\widetilde{\boldsymbol{\phi}}(\widetilde{X},t) = \boldsymbol{\phi}(X,t)$$
$$\widetilde{\boldsymbol{\nu}}(\widetilde{X},t) = \boldsymbol{\nu}(X,t). \tag{2.13}$$

Physically, we have decomposed the motion $\boldsymbol{\phi}$ into a pure rotation $\mathbf{R}(t)$ followed by the deformation $\widetilde{\boldsymbol{\phi}}$ that would be observed in the non-spinning "lab frame." Note that $\widetilde{\boldsymbol{\phi}}$ assigns to a point the location of the material particle that would be there if the body were rotating rigidly with constant angular velocity. With this change of variables, the steady spinning conditions become

$$\widetilde{\boldsymbol{\phi}}(\widetilde{X},t) = \widetilde{\boldsymbol{\phi}}(\widetilde{X},0)$$
$$\widetilde{\boldsymbol{\nu}}(\widetilde{X},t) = \widetilde{\boldsymbol{\nu}}(\widetilde{X},0) \tag{2.14}$$

for all t. Thus the steady problem has been transformed into a problem that can be solved by setting $\dot{\widetilde{\phi}}$ and $\dot{\widetilde{\nu}}$ equal to zero.

Returning to the full dynamics, we compute that $\widetilde{\phi}$ and $\widetilde{\nu}$ satisfy

$$\dot{\widetilde{\phi}} = \widetilde{\nu} - \widetilde{\mathbf{F}}\mathbf{\Omega}\widetilde{X}$$
$$\dot{\widetilde{\nu}} = \frac{1}{\rho_R}\widetilde{\mathrm{DIV}}\widetilde{\mathbf{P}_e} - \widetilde{D\widetilde{\nu}}\mathbf{\Omega}\widetilde{X}, \tag{2.15}$$

where $\widetilde{\mathbf{F}} \stackrel{\text{def}}{=} \widetilde{D}\widetilde{\phi}$, $\widetilde{\mathbf{C}} \stackrel{\text{def}}{=} \widetilde{\mathbf{F}}^{\mathsf{T}}\widetilde{\mathbf{F}}$, etc., and $\mathbf{\Omega}$ is the constant matrix

$$\mathbf{\Omega} = \dot{\mathbf{R}}\mathbf{R}^{\mathsf{T}} = \omega \begin{bmatrix} 0 & -1 \\ 1 & 0 \end{bmatrix}. \tag{2.16}$$

$\widetilde{D}$ and $\widetilde{\mathrm{DIV}}$ refer to derivatives with respect to $\widetilde{X}$. For ease of notation, we now drop the superposed tildes and refer to the transformed variables in what follows unless explicitly noted.

For later use, we also note the weak formulation of the equations of motion:

$$\int_{\mathcal{B}} \dot{\phi} \cdot \zeta = \int_{\mathcal{B}} (\nu - \mathbf{F}\mathbf{\Omega}X) \cdot \zeta$$
$$\int_{\mathcal{B}} \dot{\nu} \cdot \eta = \int_{\mathcal{B}} -\frac{1}{\rho_R}\mathbf{P}_e : D\eta - D\nu\mathbf{\Omega}X \cdot \eta. \tag{2.17}$$

Here ζ and η are arbitrary test functions, required to be $\mathbf{0}$ on the hub, Γ_h. We denote $\mathcal{G}(\phi, \nu)$ as the operator such that $(\dot{\phi}, \dot{\nu}) = \mathcal{G}(\phi, \nu)$, where $\dot{\phi}, \dot{\nu}, \phi, \nu$ satisfy (2.17).

As mentioned above, the steady spinning problem can now be written as

$$\mathbf{0} = \nu - \mathbf{F}\mathbf{\Omega}X$$
$$\mathbf{0} = \frac{1}{\rho_R}\mathrm{DIV}\,\mathbf{P}_e - D\nu\mathbf{\Omega}X \tag{2.18}$$

with boundary conditions

$$\begin{aligned} \phi(X, t) &= X & \text{on } \Gamma_h \\ \nu(X, t) &= \mathbf{\Omega}X & \text{on } \Gamma_h \\ \mathbf{P}_e\mathbf{N} &= \mathbf{0} & \text{on } \Gamma_e. \end{aligned} \tag{2.19}$$

7

In weak form the steady spinning problem can be written as

$$\mathcal{G}(\boldsymbol{\phi}, \boldsymbol{\nu}) = (\mathbf{0}, \mathbf{0}) \,. \tag{2.20}$$

When convenient, we will denote the pair $(\boldsymbol{\phi}, \boldsymbol{\nu})$ by $\mathbf{z}$. We may then write the steady state equations simply as $\mathcal{G}(\mathbf{z}) = \mathbf{0}$.

2.5. Hamiltonian structure

By virtue of our assumption of a stored energy function, the evolution of the untransformed variables is Hamiltonian, with Hamiltonian function

$$\int_{\mathcal{B}} \boldsymbol{\Psi}_e + \frac{1}{2} \rho_R \boldsymbol{\nu} \cdot \boldsymbol{\nu} \,. \tag{2.21}$$

This is a non-autonomous system due to the time-dependent boundary conditions expressing rotation of the hub. However, the evolution of the transformed variables (2.17) is an autonomous Hamiltonian system described by the following Hamiltonian:

$$\mathcal{H} = \int_{\mathcal{B}} \boldsymbol{\Psi}_e + \frac{1}{2} \rho_R \boldsymbol{\nu} \cdot \boldsymbol{\nu} - \rho_R (\mathbf{F} \boldsymbol{\Omega} X) \cdot \boldsymbol{\nu} \,. \tag{2.22}$$

Below we will discretize the equations and obtain a finite dimensional Hamiltonian system for which we can apply stability theory. In particular, let $\hat{\mathcal{H}}$ be the discretized Hamiltonian and let $\hat{\mathcal{G}}$ be the discretization of $\mathcal{G}$, which describes the motion generated by $\hat{\mathcal{H}}$: $\hat{\mathcal{G}} = (\partial \hat{\mathcal{H}} / \partial \boldsymbol{\nu}, -\partial \hat{\mathcal{H}} / \partial \boldsymbol{\phi})$. It will be useful to note that the Hessian of $\hat{\mathcal{H}}$ is related to the Jacobian of $\hat{\mathcal{G}}$ by $D\hat{\mathcal{G}} = \mathcal{J} D^2 \hat{\mathcal{H}}$, where $\mathcal{J} = \begin{bmatrix} \mathbf{0} & \mathbf{I} \\ -\mathbf{I} & \mathbf{0} \end{bmatrix}$ is skew-symmetric. Later we will use the following theorem about the stability of Hamiltonian systems: If $\mathbf{z}$ is a critical point of $\hat{\mathcal{H}}$ and the matrix $D^2 \hat{\mathcal{H}}$ is positive definite at $\mathbf{z}$, then $\mathbf{z}$ is Lyapunov stable, since energy level sets near $\hat{\mathcal{H}}(\mathbf{z})$ remain close to $\mathbf{z}$. In turn, Lyapunov stability implies that the eigenvalues of $D\hat{\mathcal{G}}$ are purely imaginary, since otherwise $\mathbf{z}$ would be linearly unstable either forward or backward in time.

3. Perturbations of the elastic model

Oden and Lin [18] numerically solved the steady state problem (2.20) in an equivalent form. Below a certain critical speed ω_c, they only observed an
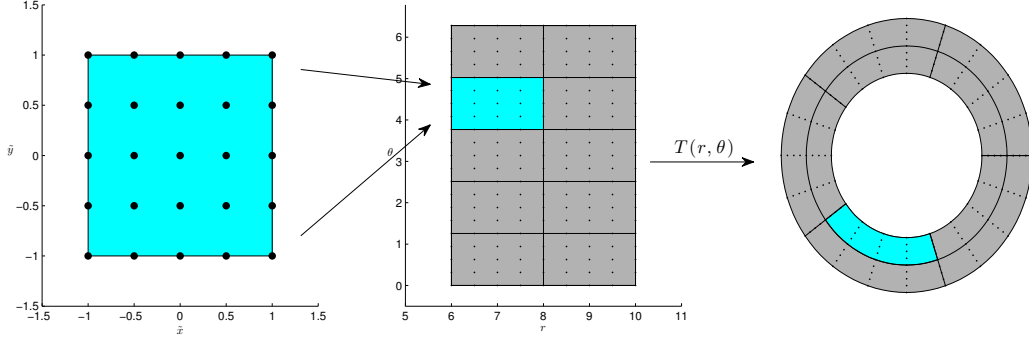
8

Figure 2: The reference element is mapped to the r-θ plane, where it is then mapped by the polar coordinate transformation exactly onto the annular reference configuration $\mathcal{B}$.

axisymmetric solution. However, for some $\omega \geq \omega_c$, they found bifurcations to non-axisymmetric solutions by noticing that the Jacobian matrix $D\mathcal{G}$ of $\mathcal{G}$ about an axisymmetric solution $\mathbf{z}$ becomes singular. We repeat this analysis but, in addition to the 0 eigenvalues studied by Oden and Lin, we also track a set of small-magnitude eigenvalues of $D\mathcal{G}$. This gives information about the behavior of the system under dynamic perturbation. In the remainder of this section, we first describe the numerical methods we employ and then describe the results of our experiments.

3.1. Numerical methods

We employ quartic quadrilateral C_0 isogeometric elements to discretize the weak equations, which in turn allows us to compute $\hat{\mathcal{G}}$, the discretization of $\mathcal{G}$ (see Fig. 2). By linearizing the weak equations about a given $\mathbf{z} = (\boldsymbol{\phi}, \boldsymbol{\nu})$, we can also compute the Jacobian matrix $D\hat{\mathcal{G}}$. When we wish to emphasize the function about which $\hat{\mathcal{G}}$ is linearized, we will write $D\hat{\mathcal{G}}[\mathbf{z}]$. We note that $D\hat{\mathcal{G}}$ can be written as the product $\mathcal{M}^{-1}\mathcal{A}$, where $\mathcal{M}$ is the mass matrix corresponding to the finite element basis. Both $\mathcal{M}$ and $\mathcal{A}$ are sparse due to the finite element formulation. We solve the steady-state equation (2.20) using Newton's method. We must perform matrix solves on $D\hat{\mathcal{G}}$, hence $\mathcal{A}$, for which we employ the direct sparse solver SuperLU [16].

To compute eigenvalues of $D\hat{\mathcal{G}}$, we employ the Arnoldi method implemented in the ARPACK software package [14]. This method works best finding large magnitude eigenvalues, so in order to find small-magnitude eigenvalues we apply it to $(D\hat{\mathcal{G}})^{-1}$. Exactly as with Newton's method, we perform matrix solves on $D\hat{\mathcal{G}}$ using SuperLU.

3.2. Results: Classic modes

We first state our choice of units and choice of constants. Our units are Newtons (N), megagrams (Mg), and seconds (s). This choice implies our unit for length is millimeters (mm). Our body has inner radius $r_1 = 240$mm and outer radius $r_2 = 400$mm. The density of the body is $\rho = 1 \times 10^{-9}$ Mg/mm^3. The bulk modulus κ and shear modulus μ are 689 N/mm^2 and 6.89 N/mm^2, respectively, and we set $s = 0.5$.

We briefly recall the results of Oden and Lin in some detail. For any rotation speed ω, they found an axisymmetric solution $\mathbf{z}_\omega$. For small ω they observed $D\hat{\mathcal{G}}[\mathbf{z}_\omega]$ is non-singular, but at a speed ω_c they observed that $D\hat{\mathcal{G}}[\mathbf{z}_\omega]$ became highly singular, i.e. $D\hat{\mathcal{G}}[\mathbf{z}_\omega]$ had a large dimensional nullspace. For $\omega > \omega_c$, they observed discrete speeds ω_i, $3 \leq i < \infty$, where $D\hat{\mathcal{G}}[\mathbf{z}_{\omega_i}]$ also became singular. Perturbing away from the axisymmetric solution in the direction of a null vector of $D\hat{\mathcal{G}}[\mathbf{z}_{\omega_i}]$ led to an i-peak standing wave solution to the steady spinning problem. They noted that the ω_i decrease monotonically and limit to ω_c from above. Thus Oden and Lin discovered a hierarchy of i-peak standing wave solutions.

Using ARPACK, we additionally compute the smallest eigenvalues of the matrix $D\hat{\mathcal{G}}[\mathbf{z}_\omega]$ for a range of values of ω and plot them in Fig. 3. When $\omega < \omega_c$, the eigenvalues are all purely imaginary. This is explained by the Hamiltonian structure of the problem. When $\omega = 0$, the axisymmetric solution is the identity configuration and we can directly compute that $D^2\hat{\mathcal{H}}$ is positive definite. As we increase ω to ω_c, we numerically observe that $D^2\hat{\mathcal{H}}$ remains non-singular, hence positive definite. Thus we expect that the eigenvalues of $D\hat{\mathcal{G}}$ are purely imaginary, which our eigenvalue computations confirm. For $\omega \geq \omega_c$, we do not necessarily expect purely imaginary eigenvalues, and in fact we do observe eigenvalues with real components in this regime, although they appear to be spurious as explained below.

In the plot on the left of Fig. 3, we can see the smallest eigenvalues are bounded away from 0 initially and then rapidly move toward 0. Where they collide with 0 indicates $D\hat{\mathcal{G}}[\mathbf{z}_\omega]$ has a loss of rank and identifies ω_c. The plot on the right of Fig. 3 is a zoomed-in portion of the plot on the left. There we can see a series of Xs that increase in frequency as we approach $\omega_c \approx 210$ rad/s from the right. These Xs correspond to the i-peak standing wave solutions found by Oden and Lin. The Xs cross zero at the bifurcation speeds ω_i where $D\hat{\mathcal{G}}[\mathbf{z}_\omega]$ is singular. The sporadic eigenvalues not lying on an X appear to be caused by the discretization of the equations and do not persist when the mesh is refined. Occasionally these (sporadic) eigenvalues
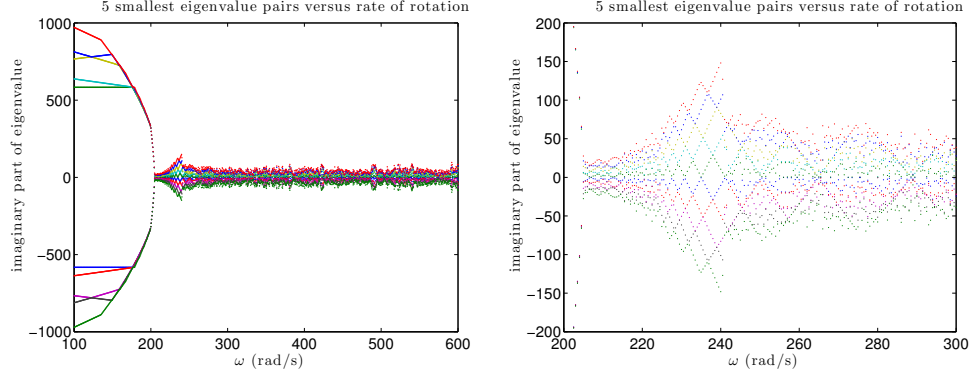
10

Figure 3: Plots of the smallest eigenvalues of $D\hat{\mathcal{G}}[\mathbf{z}_\omega]$. Here ω_c is near 210 rad/s and a mesh with 8 radial elements and 64 angular elements has been used.
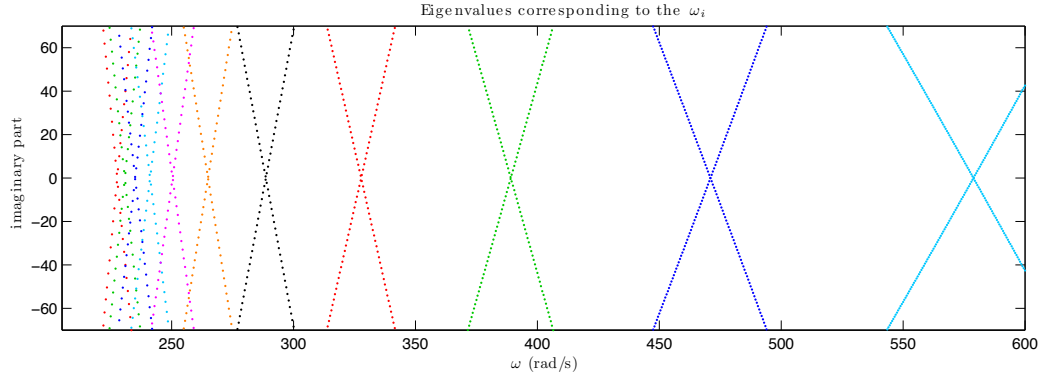

Figure 4: Plot of the λ_i and $\bar{\lambda}_i$. The leftmost X corresponds to λ_{12} while the rightmost X corresponds to λ_2.

will have a non-zero real component, but we did not observe any of these eigenvalues with corresponding eigenvectors that were resolved by our mesh. If we plot only the eigenvalues that correspond to the ω_i, $i = 2, \ldots, 12$, we obtain Fig. 4. We will denote these eigenvalues as $\lambda_i(\omega)$ with complex conjugate $\bar{\lambda}_i(\omega)$. Note that $\lambda_i(\omega_i) = 0$. For each λ_i and $\bar{\lambda}_i$ there is a complex conjugate pair of eigenvectors. We will denote the eigenvector associated with λ_i by $\mathbf{e}_i(\omega)$. The real $\boldsymbol{\phi}$ components of two of the $\mathbf{e}_i$ are plotted in Fig. 5.

11

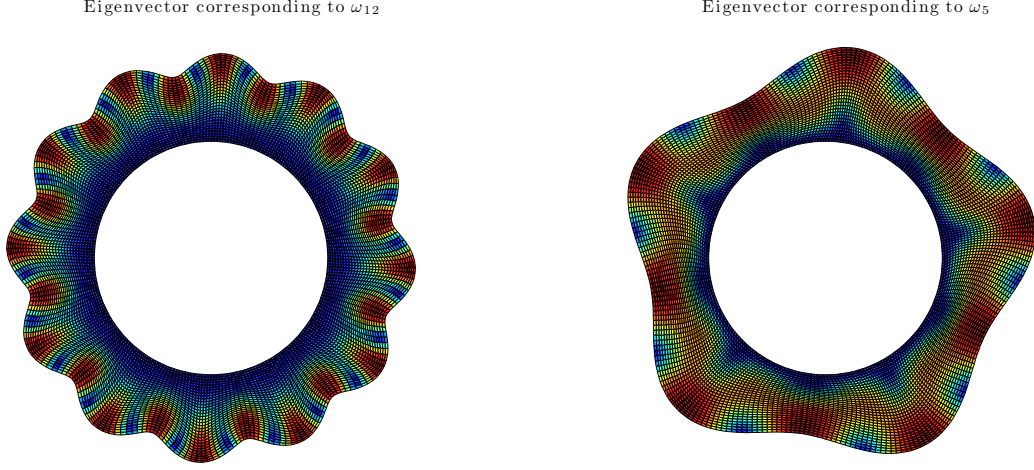Eigenvector corresponding to ω_{12} Eigenvector corresponding to ω_5

Figure 5: Plot of the real ϕ component of $\mathbf{e}_{12}$ and $\mathbf{e}_5$. The plots are colored according to the norm of the real ϕ component, with red being large and blue small.

3.3. Results: Radial hierarchy

In addition to the standing wave eigenvectors with i peaks we discovered other eigenvectors which correspond to other bifurcation speeds. We plot these eigenvectors in Fig. 6 and note that these eigenvectors have more complexity in the radial direction than the eigenvectors discussed by Oden and Lin. To investigate this, we note that the rotational symmetry of our problem implies that eigenvectors must have a certain form. $D\mathcal{G}$ commutes with a family of rotation operators $\mathcal{R}(\alpha)$ defined by

$$\mathcal{R}(\alpha)\left(\begin{array}{c}\bar{\phi}\\\bar{\nu}\end{array}\right)(X) = \left(\begin{array}{c}\mathbf{R}(\alpha)\bar{\phi}(\mathbf{R}^{\mathsf{T}}(\alpha)X)\\\mathbf{R}(\alpha)\bar{\nu}(\mathbf{R}^{\mathsf{T}}(\alpha)X)\end{array}\right). \tag{3.1}$$

Hence any eigenvector $\bar{\mathbf{z}} = (\bar{\phi}, \bar{\nu})$ of $D\mathcal{G}$ associated to a distinct eigenvalue must also be an eigenvector of $\mathcal{R}(\alpha)$ for all α. This implies that $\bar{\mathbf{z}} = (\bar{\phi}, \bar{\nu})$, written as a function of polar coordinates, is of the form

$$\begin{aligned}\bar{\phi}(r,\theta) &= a_1(r)e^{\mathfrak{i}(k+1)\theta}\left[\begin{array}{c}1\\\mathfrak{i}\end{array}\right] + a_2(r)e^{\mathfrak{i}(k-1)\theta}\left[\begin{array}{c}1\\-\mathfrak{i}\end{array}\right],\\\bar{\nu}(r,\theta) &= a_3(r)e^{\mathfrak{i}(k+1)\theta}\left[\begin{array}{c}1\\\mathfrak{i}\end{array}\right] + a_4(r)e^{\mathfrak{i}(k-1)\theta}\left[\begin{array}{c}1\\-\mathfrak{i}\end{array}\right].\end{aligned} \tag{3.2}$$

Here, $\mathfrak{i} = \sqrt{-1}$, k is a fixed integer, and the $a_i(r)$ are functions that depend only on the radial coordinate r. In particular, the above eigenfunction is
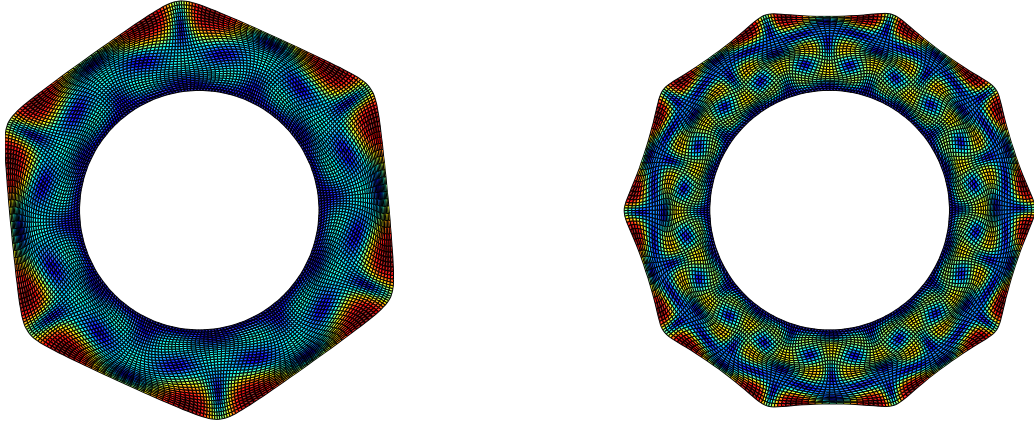
Figure 6: Plot of the real ϕ component of eigenvectors outside of the N-peak hierarchy discovered by Oden and Lin. The plots are colored according to the displacement from the reference configuration, with red being high displacement and blue being little displacement.

invariant with respect to $\mathcal{R}(\alpha)$ for $\alpha = 2\pi n/k$ and, hence, the standing wave solutions with N peaks must be in the above form with $k = N$ or $k = -N$.

Given a numerically computed eigenvector with N peaks, we can compute its Fourier series in the θ direction. As expected due to (3.2), we observe exactly two Fourier modes: $N \pm 1$ or $-N \pm 1$. We repeat this computation for each value of r to determine the functions $a_i(r)$. By plotting the a_i we can compare the radial complexity of different eigenvectors. As in the upper left plot in Fig. 7, we observe the $a_i(r)$ corresponding to the $\mathbf{e}_i$ have one local extremum. The $a_i(r)$ corresponding to other eigenvectors have more radial complexity with $2, 3, 4$ or more local extrema.

Examining these solutions, we find an entire N-peak hierarchy of eigenfunctions with a_i having two local extrema. We denote these eigenvectors as $\mathbf{e}_{i,2}$ with corresponding eigenvalues and bifurcation speeds denoted by $\lambda_{i,2}$ and $\omega_{i,2}$, respectively. Fig. 8 shows the corresponding paths of their eigenvalues. As in Figs. 6 and 7, we also found eigenvalues with more radial complexity than the $\mathbf{e}_{i,2}$, which suggests that the standing wave solutions may be described by a two-dimensional hierarchy $\mathbf{e}_{i,j}$, where i is the number of peaks in the circumferential direction and j is the number of oscillations in the radial direction. It is an unresolved question whether the $\omega_{i,j}$ converge to ω_c as $i \to \infty$ for fixed j, or if perhaps there is a distinct critical speed for each j.
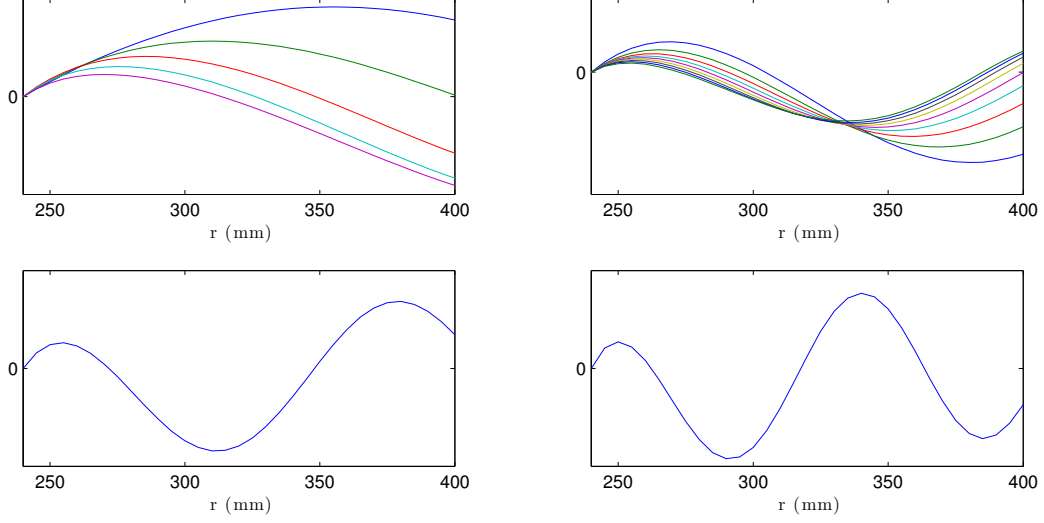
Figure 7: Plots of the real part of a_1 for various eigenvectors. The top left plot corresponds to the $\mathbf{e}_i$. The top right plot corresponds to N-peak bifurcations with extra radial complexity. The bottom plots correspond to eigenvectors with even greater radial complexity.
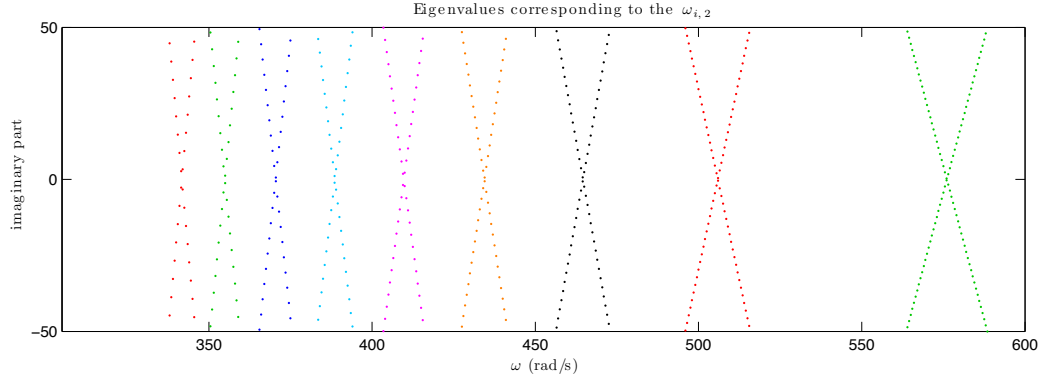

Figure 8: Plot of the $\lambda_{i,2}$ and $\bar{\lambda}_{i,2}$. The leftmost X corresponds to $\lambda_{12,2}$ while the rightmost X corresponds to $\lambda_{4,2}$.

14

We note that in their monograph [22], Oden and Rabier discovered analytically a two-dimensional hierarchy of eigenvalues $\zeta_{i,j}$ of an operator related to $D\mathcal{G}$. However, their analysis was not able to show that the $\zeta_{i,j}$ corresponded to eigenvalues of $D\mathcal{G}$ for $j > 1$ and it applied only to incompressible hyperelastic materials. Incompressibility prevents solutions on the trivial branch of stationary solutions from expanding radially, but does enable the use of potential functions to describe the solutions on other branches.

4. Viscoelastic effects

In §3, we presented the classical stability analysis of a spinning body along with a discussion of an additional hierarchy of bifurcation modes not reported on to date. The classical analysis is, however, restricted to the elastic setting. In this section, we consider the influence of viscoelasticity on the stability of a spinning body and, in particular, we discuss the influence of the choice of the (finite deformation) viscoelastic model.

Two common viscoelastic models are the linear model proposed by Simo [26] and the nonlinear Sidoroff [25] model as detailed by Reese and Govindjee [12, 24, 23]. In both models, additional variables are introduced that govern a viscoelastic component of the first Piola-Kirchhoff stress tensor, which we denote $\mathbf{P}_v$. The equations of motion are then driven by the total Piola-Kirchhoff stress tensor $\mathbf{P}_{total} = \mathbf{P}_e + \mathbf{P}_v$. We briefly describe the two models below. For the purpose of describing the models in a general context, we will revert to using $\boldsymbol{\phi}$, $\boldsymbol{\nu}$, $\mathbf{F}$, etc. as the untransformed variables and $\widetilde{\boldsymbol{\phi}}$, $\widetilde{\boldsymbol{\nu}}$, $\widetilde{\mathbf{F}}$, etc. as the transformed variables.

4.1. Linear viscoelastic model

We refer to the model of Simo [26] as a linear model because the evolution of the viscoelastic variables can be described by a differential equation that is linear in the viscoelastic variables – even though it was designed to be applied to finite deformation problems.

The model is often presented by first introducing a viscoelastic (over-)stress tensor $\mathbf{Q}$ defined by the convolution equation

$$\mathbf{Q}(t) = \int_{-\infty}^{t} \exp\left(\frac{-(t-s)}{\tau}\right) \frac{d}{ds}\left(\mathbf{S}_e(s)\right) dt. \tag{4.1}$$

Here $\mathbf{S}_e = \mathbf{F}^{-1}\mathbf{P}_e$ is the second Piola-Kirchhoff stress tensor corresponding to $\mathbf{P}_e$ and τ is the viscoelastic relaxation time. Differentiating (4.1) yields

an evolution equation for $\mathbf{Q}$:

$$\dot{\mathbf{Q}}(t) = -\frac{1}{\tau}\mathbf{Q}(t) + \dot{\mathbf{S}}_e(t)\,. \tag{4.2}$$

Note that the evolution depends linearly on $\mathbf{Q}$. Given $\mathbf{Q}$, we define a viscoelastic second Piola-Kirchhoff stress tensor $\mathbf{S}_v$ by $\mathbf{S}_v = \nu\mathbf{Q}$, where ν is a weight parameter describing the strength of the viscoelastic response. We then define $\mathbf{P}_v = \mathbf{FS}_v$.

4.2. Nonlinear viscoelastic model

The nonlinear Sidoroff viscoelastic model of Reese and Govindjee [12, 24, 23] is derived by assuming a multiplicative split of the deformation gradient

$$\mathbf{F} = \mathbf{F}_e\mathbf{F}_v \tag{4.3}$$

into an elastic part $\mathbf{F}_e$ and a viscous part $\mathbf{F}_v$. In addition, we assume that the total free energy is given as a sum of the elastic energy $\mathbf{\Psi}_e(\mathbf{C})$ described above and a viscoelastic energy $\mathbf{\Psi}_v(\mathbf{C}_e)$ which only depends on the strain associated with the elastic deformation: $\mathbf{C}_e = \mathbf{F}_e^\mathsf{T}\mathbf{F}_e$. In the case of isotropy, $\mathbf{\Psi}_v$ can also be written as depending on the elastic left Cauchy-Green tensor $\mathbf{b}_e = \mathbf{F}_e\mathbf{F}_e^\mathsf{T}$, which yields a more convenient formulation. We define $\mathbf{\Psi}_v(\mathbf{b}_e)$ similarly to $\mathbf{\Psi}_e$:

$$\mathbf{\Psi}_v = \nu\left(\frac{\kappa}{4}\left(I_3^e - \log I_3^e - 1\right) + \frac{\mu}{2}(1-s)\left(I_1^e - \log I_3^e - 3\right) + \frac{\mu}{2}s\left(I_2^e - 2\log I_3^e - 3\right)\right), \tag{4.4}$$

where I_1^e, I_2^e, I_e^e are the invariants of the three-dimensional tensor $\mathbf{b}_{3e} = \begin{bmatrix} \mathbf{b}_e & 0 \\ 0 & 1 \end{bmatrix}$. $\mathbf{P}_v$ is now given by

$$\begin{aligned}
\mathbf{P}_v &= 2\frac{\partial\mathbf{\Psi}_v}{\partial\mathbf{b}_e}\mathbf{b}_e\mathbf{F}^{-\mathsf{T}} \\
&= \nu\left(\frac{\kappa}{2}(I_3^e - 1)\mathbf{I} + \mu(1-s)(\mathbf{b}_e - \mathbf{I}) + \mu s(I_1^e\mathbf{b}_e - \mathbf{b}_e^2 - 2\mathbf{I})\right)\mathbf{F}^{-\mathsf{T}}\,.
\end{aligned} \tag{4.5}$$

The model is completed by giving an evolution equation for $\mathbf{b}_e$:

$$\dot{\mathbf{b}_e} = \boldsymbol{\ell}\mathbf{b}_e + \mathbf{b}_e\boldsymbol{\ell}^\mathsf{T} - 2\mathcal{V}(\boldsymbol{\tau}_e)\mathbf{b}_e\,, \tag{4.6}$$

16

where

$$\boldsymbol{\ell} = \dot{\mathbf{F}}\mathbf{F}^{-1}$$

$$\boldsymbol{\tau}_e = 2\frac{\partial \boldsymbol{\Psi}_v}{\partial \mathbf{b}_e}\mathbf{b}_e \qquad (4.7)$$

$$\mathcal{V}(\boldsymbol{\tau}_e) = C_1\left(\boldsymbol{\tau}_e - \frac{1}{2}(\operatorname{tr}\boldsymbol{\tau}_e)\mathbf{I}\right) + C_2\frac{1}{2}(\operatorname{tr}\boldsymbol{\tau}_e)\mathbf{I}, \qquad C_1, C_2 > 0.$$

Reese and Govindjee [24] have proved that the Clausius-Duhem inequality is satisfied for their nonlinear viscoelastic model:

$$\frac{1}{2}\mathbf{S} : \dot{\mathbf{C}} - \dot{\boldsymbol{\Psi}}_{total} \geq 0, \qquad (4.8)$$

but noted that it is unknown whether the linear viscoelastic model of [26] satisfies this inequality for any appropriate free energy function.

4.3. Steady state spinning of a viscoelastic body

We now derive steady spinning conditions for the viscoelastic variables $\mathbf{Q}$ and $\mathbf{b}_e$. Recall that steady spinning motion of an elastic body is given by

$$\boldsymbol{\phi}(X,t) = \boldsymbol{\phi}(\mathbf{R}(t)X,0)$$
$$\boldsymbol{\nu}(X,t) = \boldsymbol{\nu}(\mathbf{R}(t)X,0). \qquad (4.9)$$

The same relationship should hold for any scalar, vector, or tensor quantity defined on the deformed configuration; in particular it should hold for the left Cauchy-Green deformation tensor $\mathbf{b} = \mathbf{F}\mathbf{F}^\mathsf{T}$. Since $\mathbf{b}_e$ is analogous to $\mathbf{b}$, we require $\mathbf{b}_e$ to satisfy

$$\mathbf{b}_e(X,t) = \mathbf{b}_e(\mathbf{R}X,0), \qquad (4.10)$$

where we omit t in the notation for $\mathbf{R}(t)$ in this section. The relationship for other quantities can be determined by using $\mathbf{F}$ to push them onto the deformed configuration. We compute from (4.9) that $\mathbf{F}$ satisfies

$$\mathbf{F}(X,t) = \mathbf{F}(\mathbf{R}X,0)\mathbf{R}. \qquad (4.11)$$

Using this and the integral definition of $\mathbf{Q}$ in (4.1), we find that $\mathbf{Q}$ satisfies

$$\mathbf{R}\mathbf{Q}(X,t)\mathbf{R}^\mathsf{T} = \mathbf{Q}(\mathbf{R}X,0). \qquad (4.12)$$

17

We then define the transformed variables

$$\widetilde{\mathbf{Q}}(\widetilde{X}, t) = \mathbf{R}\mathbf{Q}(X, t)\mathbf{R}^{\mathsf{T}}$$
$$\widetilde{\mathbf{b}}_e(\widetilde{X}, t) = \mathbf{b}_e(X, t) \,. \tag{4.13}$$

A computation shows that they evolve as

$$\dot{\widetilde{\mathbf{Q}}} = -\frac{1}{\tau}\widetilde{\mathbf{Q}}(t) + \dot{\widetilde{\mathbf{S}}}_e(t) + \mathbf{\Omega}\widetilde{\mathbf{Q}} - \widetilde{\mathbf{Q}}\mathbf{\Omega} - \widetilde{D}\widetilde{\mathbf{Q}}\mathbf{\Omega}\widetilde{X}$$
$$\dot{\widetilde{\mathbf{b}}}_e = \widetilde{\boldsymbol{\ell}}\widetilde{\mathbf{b}}_e + \widetilde{\mathbf{b}}_e\widetilde{\boldsymbol{\ell}}^{\mathsf{T}} - 2\mathcal{V}(\widetilde{\boldsymbol{\tau}}_e)\widetilde{\mathbf{b}}_e - \widetilde{D}\widetilde{\mathbf{b}}_e\mathbf{\Omega}\widetilde{X} \,. \tag{4.14}$$

Again, we now drop the superposed tildes and will only refer to the transformed variables below. The weak formulations of the equations of motion for $\boldsymbol{\phi}$ and $\boldsymbol{\nu}$ become

$$\int_{\mathcal{B}} \dot{\boldsymbol{\phi}} \cdot \zeta = \int_{\mathcal{B}} (\boldsymbol{\nu} - \mathbf{F}\mathbf{\Omega}X) \cdot \zeta$$
$$\int_{\mathcal{B}} \dot{\boldsymbol{\nu}} \cdot \eta = \int_{\mathcal{B}} -\frac{1}{\rho_R}\mathbf{P}_{total} : D\eta - D\boldsymbol{\nu}\mathbf{\Omega}X \cdot \eta \,. \tag{4.15}$$

The only difference from (2.17) being that $\mathbf{P}_e$ is replaced with $\mathbf{P}_{total}$. This is then coupled with either the linear viscoelastic model

$$\int_{\mathcal{B}} \dot{\mathbf{Q}} : K = \int_{\mathcal{B}} \left(-\frac{1}{\tau}\mathbf{Q}(t) + \dot{\mathbf{S}}_e(t) + \mathbf{\Omega}\mathbf{Q} - \mathbf{Q}\mathbf{\Omega} - D\mathbf{Q}\mathbf{\Omega}X \right) : K \,, \quad (4.16)$$

or the nonlinear viscoelastic model

$$\int_{\mathcal{B}} \dot{\mathbf{b}}_e : K = \int_{\mathcal{B}} \left(\boldsymbol{\ell}\mathbf{b}_e + \mathbf{b}_e\boldsymbol{\ell}^{\mathsf{T}} - 2\mathcal{V}(\boldsymbol{\tau}_e)\mathbf{b}_e - D\mathbf{b}_e\mathbf{\Omega}X \right) : K \,. \tag{4.17}$$

Here K is an arbitrary symmetric tensor-valued test function. For later use, we define $\hat{\mathcal{G}}_{vq}, \hat{\mathcal{G}}_{vb}$ to be the discretized differential operators corresponding to the linear and nonlinear viscoelastic models, respectively. We will write $\mathbf{z}^{vq}$ for the triple $(\boldsymbol{\phi}, \boldsymbol{\nu}, \mathbf{Q})$ and $\mathbf{z}^{vb}$ for $(\boldsymbol{\phi}, \boldsymbol{\nu}, \mathbf{b}_e)$.

The structure of $\hat{\mathcal{G}}_{vb}$ is similar in form to that of LeTallec and Rahier [15], who also utilized a Sidoroff viscoelastic model in their spinning study. However the structure of $\hat{\mathcal{G}}_{vq}$ differs from other rolling studies that use convolution based models [18, 10, 11]. In particular, we treat $\mathbf{Q}$ as an independent field variable. While this increases the number of global unknowns, it avoids well-known issues associated with the accurate computation of $\mathbf{Q}$ at the Gauss points in a finite element computation as well as with the accurate computation of $D\hat{\mathcal{G}}_{vq}$; see for example [11, 17].
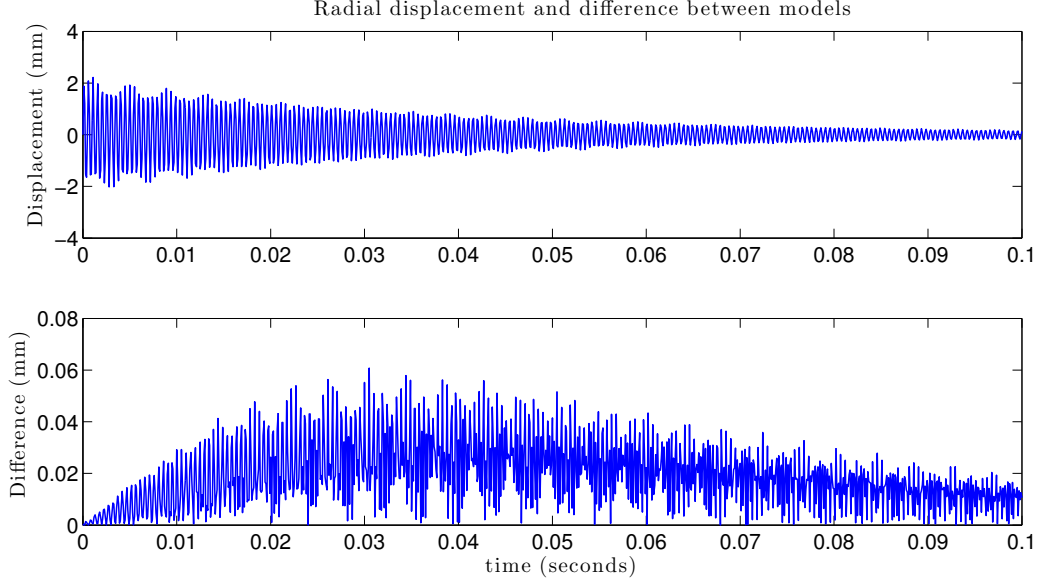
Figure 9: The top plot shows the radial displacement on the edge of the body for an expanding initial state for the two viscoelasticity models. The bottom plot shows the difference between the models, which is several orders of magnitude smaller than the displacement. As a result, only a single curve can be seen in the top panel.

5. Perturbations of the viscoelastic models

We repeat the experiments of §3 with the viscoelastic models. The numerical framework changes very little. We model the viscoelastic variables using the same finite element framework and apply Newton's method to solve $\hat{\mathcal{G}}_{vq} = \mathbf{0}$ or $\hat{\mathcal{G}}_{vb} = \mathbf{0}$. The values of the viscoelastic parameters are $\nu = 1$ and $\tau = 0.01$ seconds. We choose the constants C_1 and C_2 to be $1/(2\kappa\tau)$ and $1/(2\mu\tau)$, respectively, in order to match the relaxation responses of the linear and nonlinear viscoelastic models at small to modest deformations. To illustrate the quality of the match obtained with our parameter selection heuristics, in Figs. 9 and 10 we compare the models' transient relaxation response to initial conditions that excite shear and compression modes, respectively. The differences in the relaxation behavior are seen to be quite minor.

5.1. Results: Steady viscoelastic spinning

We begin by considering the linear viscoelastic model. As with the elastic case, we find a single radially symmetric solution $\mathbf{z}_\omega^{vq}$ for any body speed ω.
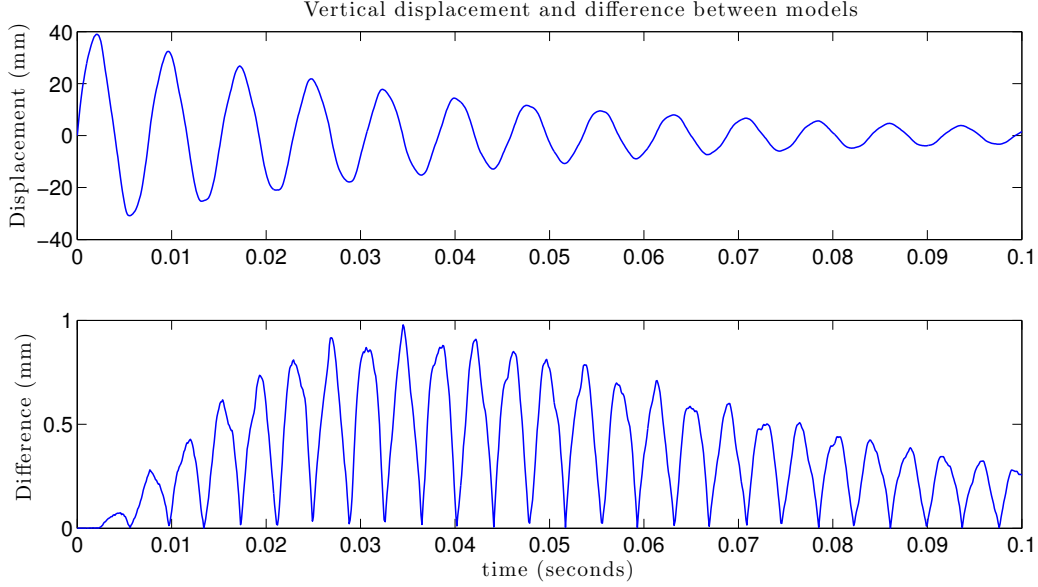
19

Figure 10: The top plot shows the vertical displacements on the rightmost edge of the body for a twisting initial state. The bottom plot shows the difference between the models. This difference is small enough that only a single curve can be seen in the top plot.

We compute the eigenvalues of the operator $\hat{\mathcal{G}}_{vq}[\mathbf{z}_{\omega}^{vq}]$, which we plot in Fig. 11.

A major difference between the eigenvalues in the elastic case (as in Fig. 3), is that the Hamiltonian structure is destroyed and we no longer expect purely imaginary eigenvalues. In fact, all of the eigenvalues we observe have a real component. Moreover, there were no eigenvalues passing through 0, and the matrix $\hat{\mathcal{G}}_{vq}[\mathbf{z}_{\omega}^{vq}]$ always remains non-singular. Thus we find no bifurcation speeds that lead to other steady state solutions. Yet there is still an event analogous to the critical bifurcation speed ω_c at which point many eigenvalues approach 0, although they do not pass through 0. We will call this speed ω_c^{vq}, which is approximately 285 rad/s.

We plot a set of the smallest magnitude eigenvalues in Fig. 12, and obtain a very similar picture to Fig. 4, with the addition of a real component. We observe that there are eigenvalues of $\hat{\mathcal{G}}_{vq}[\mathbf{z}_{\omega}^{vq}]$ which have a structure analogous to the λ_i of the elastic case. We will denote these eigenvalues $\lambda_i^{vq}(\omega)$. By "analogous", we mean that the imaginary parts of the λ_i^{vq} form Xs and the corresponding eigenvector, denoted $\mathbf{e}_i^{vq}$, has a similar structure to the $\mathbf{e}_i$. We
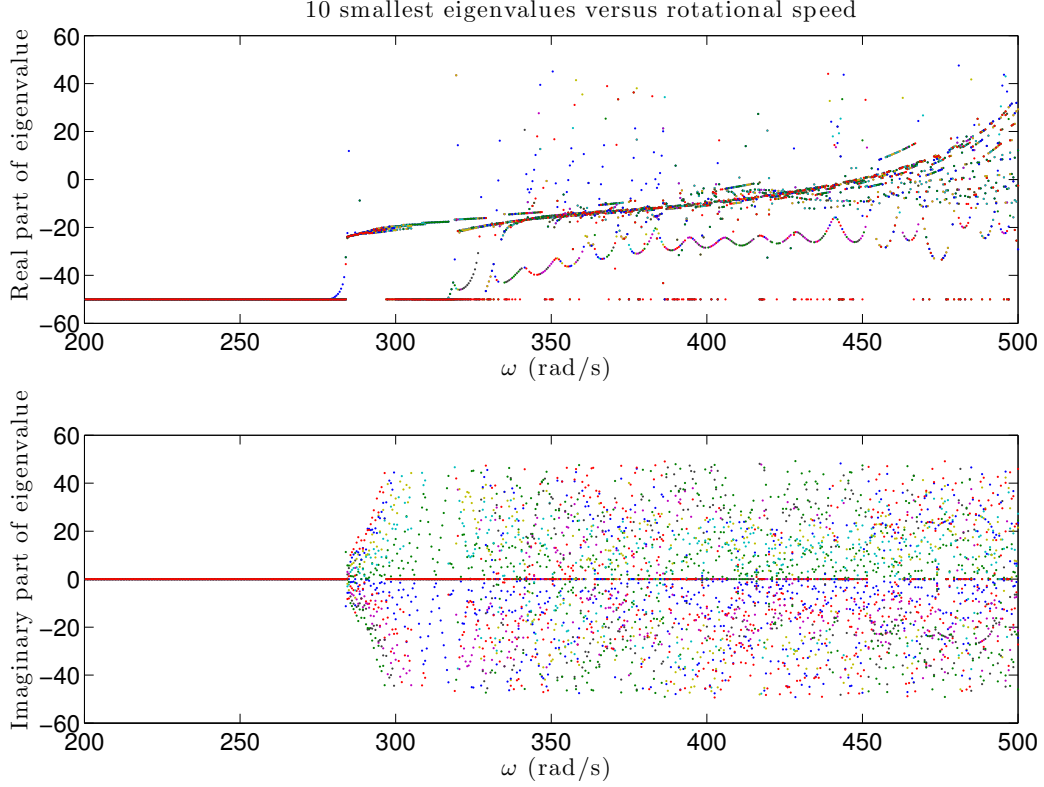
20

Figure 11: Plots of the smallest eigenvalues of $\hat{\mathcal{G}}_{vq}[\mathbf{z}_{\omega}^{vq}]$. Here ω_c^{vq} is near 285 rad/s.

will call ω_i^{vq} the speed at which $\mathrm{Im}\,\lambda_i^{vq}(\omega) = 0$. However, the ω_i^{vq} are not bifurcation speeds, since the λ_i^{vq} have a non-zero real component, so we will refer to them as pseudo-bifurcation speeds.

As in the elastic case of §3.3, we can observe eigenvectors and eigenvalues that correspond to the second hierarchy of standing waves; i.e. eigenvectors of the second hierarchy persist in the viscoelastic case and suggest, here also, there is a two-dimensional hierarchy $\mathbf{e}_{i,j}^{vq}$.

When we examine the nonlinear viscoelastic model, we see similar results in the sense that the eigenvalues λ_i^{vb} (with corresponding eigenvectors denoted $\mathbf{e}_i^{vb}$) have a real component; $\hat{\mathcal{G}}_{vb}$ remains non-singular; there is critical speed ω_c^{vb} (near 290 rad/s); and the eigenvectors outside of Oden and Lin's i-peak hierarchy remain. Fig. 13 shows the trajectories of the λ_i^{vb} when ω is varied. Notice, however, that there is one major difference between the linear and nonlinear model – viz., the real parts of the λ_i^{vq} steadily increase
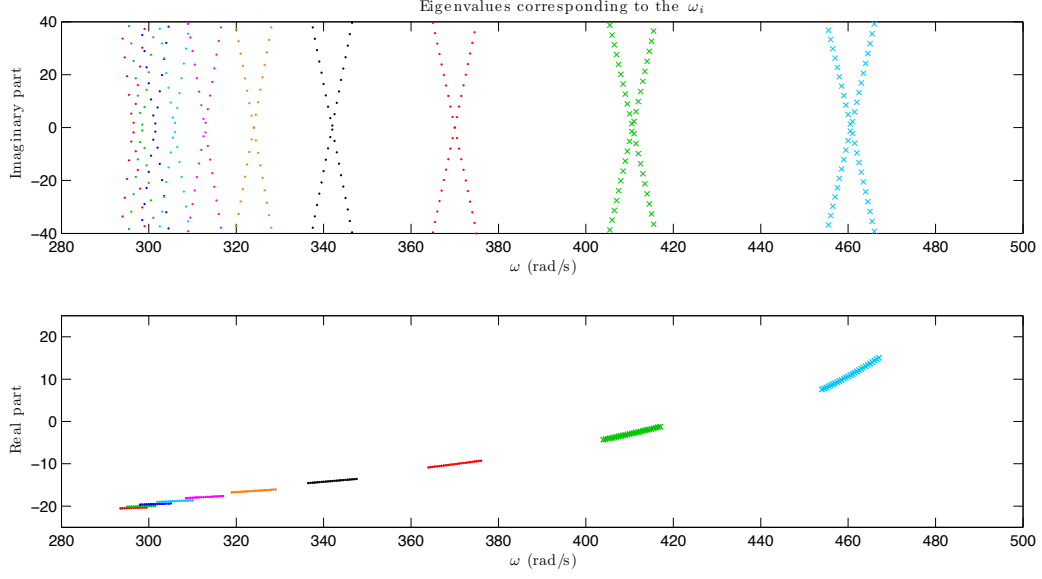
Figure 12: Plot of the real and imaginary components of the λ_i^{vq}. The leftmost X corresponds to λ_{12}^{vq} while the rightmost X corresponds to λ_3^{vq}.
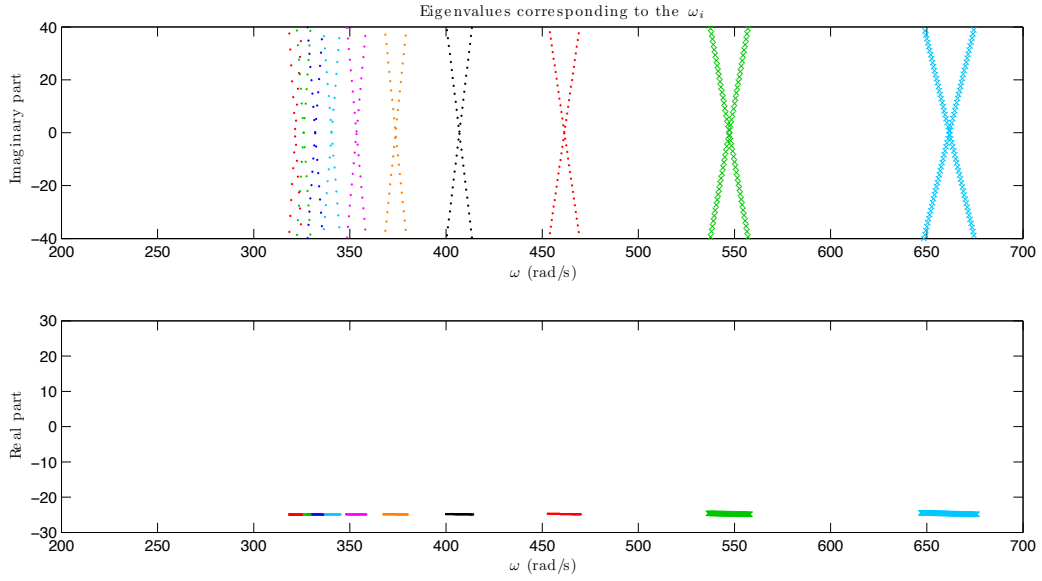

Figure 13: Plot of the real and imaginary components of the λ_i^{vb}. The leftmost X corresponds to λ_{12}^{vb} while the rightmost X corresponds to λ_3^{vb}.
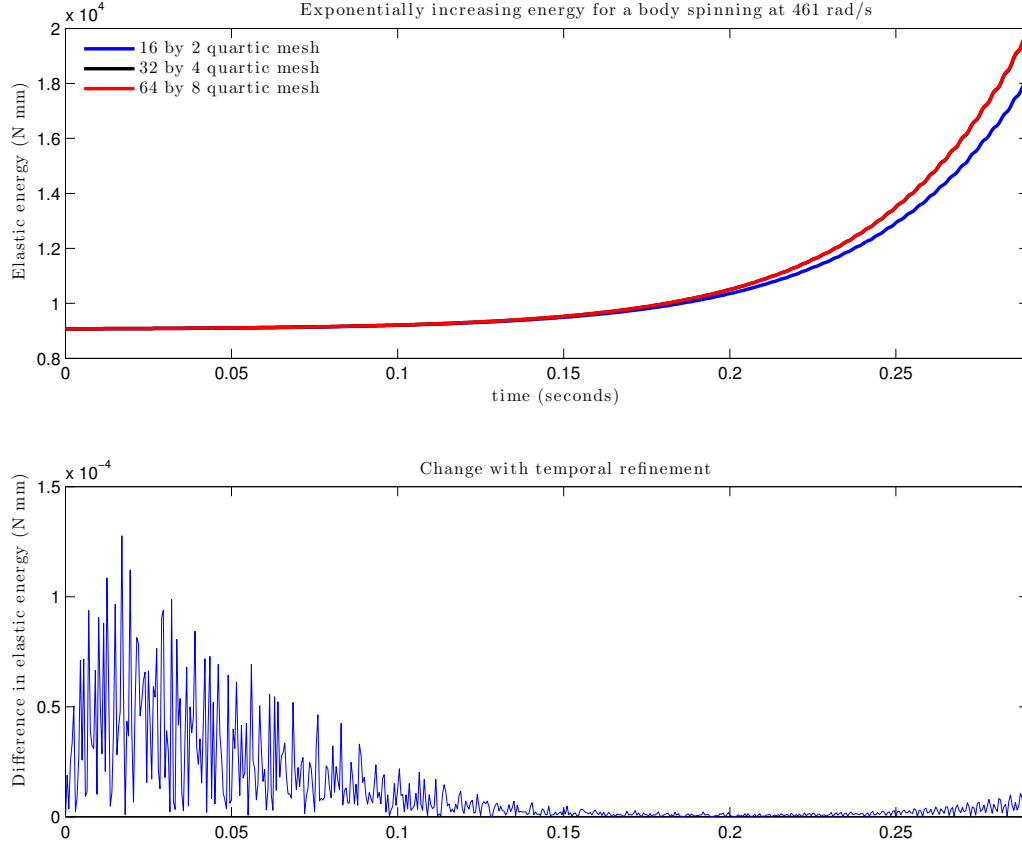
Figure 14: The upper plot shows the elastic energy for the steady state solution of the linear viscoelastic model perturbed in the direction of $\mathrm{Re}\{\mathbf{e}_3^{vq}\}$. We repeat the calculation for three mesh sizes. The discrepancy between the finer meshes is barely visible on the plot. The lower plot shows the difference when halving the time step for the finest mesh.

as ω increases while the real parts of the λ_i^{vb} remain level (see Figs. 12 and 13). We investigate this crucial difference in the next section.

6. Stability of the viscoelastic models

For large enough ω we observe from Fig. 12 that λ_3^{vq} has a positive real part, which indicates an unstable mode of the stationary solution for the linear viscoelastic model. To examine further, we perturb the stationary solution corresponding to rotational speed $\omega_3^{vq} \approx 461$ rad/s in the direction $\mathrm{Re}\{\mathbf{e}_3^{vq}\}$ and allow the body to evolve in time according to the nonlinear
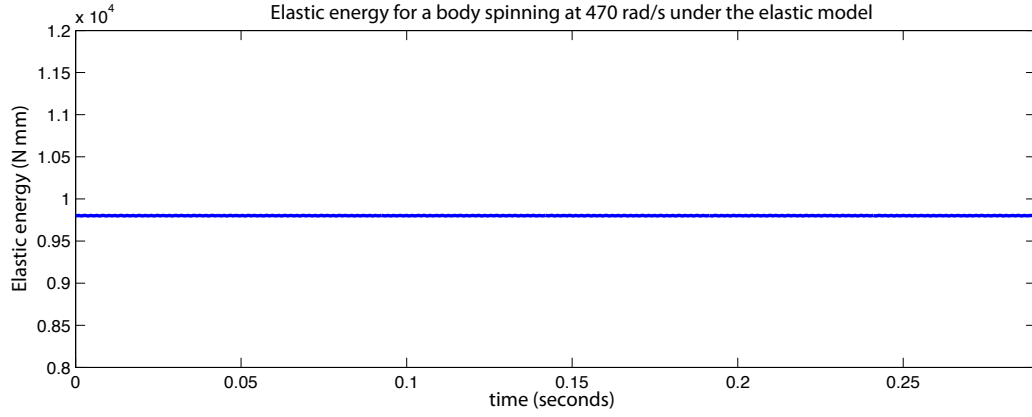
23

Figure 15: We plot the elastic energy for the steady-state solution of the elastic model perturbed in the direction of $\mathrm{Re}\{\mathbf{e}_3\}$. Unlike the linear viscoelastic case, the elastic energy does not increase.
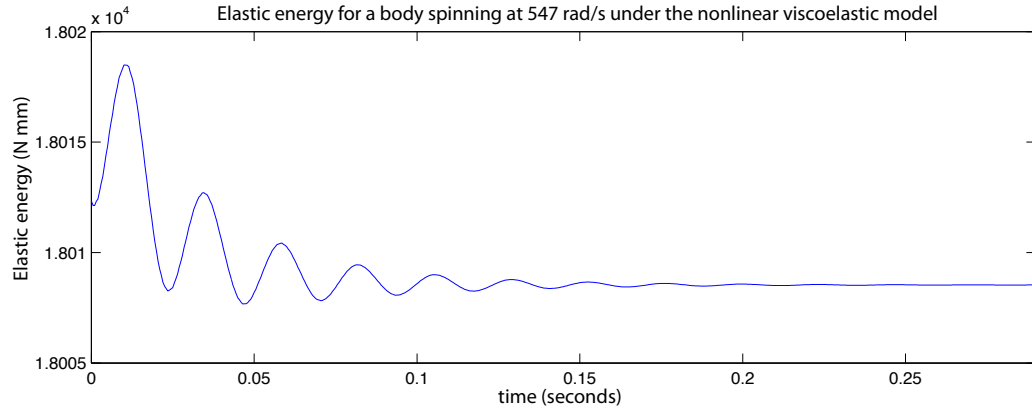

Figure 16: We plot the elastic energy for the same spinning initial condition as in Fig. 14, but using the nonlinear model of viscoelasticity perturbed in the direction $\mathrm{Re}\{\mathbf{e}_3^{vb}\}$. Unlike the linear viscoelastic model case, the elastic energy does not increase, on average.

dynamics with this initial configuration using an 8th order Runge-Kutta time-stepping scheme [9]. Choosing the real part keeps the calculation real, and boils down to selecting an arbitrary phase in the oscillatory part of the linearized solution associated with the unstable eigenvalue. The idea is to seed the nonlinear evolution with an unstable linearized mode, so the phase is unimportant. Counter to the common intuition surrounding viscoelastic response, we observe the system exponentially gain energy to the point that our numerical time-stepper returned NaNs. We observe the same phenomenon with any initial condition evolved at rotation speeds greater than approximately 420 rad/s.

Figure 14 shows the exponential increase in elastic energy with time. To ensure that this non-physical behavior of the linear viscoelastic model was not caused by any numerical issues, Fig. 14 shows the energy versus time curves for several mesh sizes and for two different time-step sizes. The results indicate that the model response has been fully resolved and, thus, that the instability is intrinsic to the model. We also repeated the experiment with the elastic model and nonlinear viscoelastic models using analogous initial conditions: $\mathbf{z}_\omega$ was perturbed in the direction $\text{Re}\{\mathbf{e}_3\}$ with speed $\omega = 470$ rad/s $\approx \omega_3$ for the elastic model and $\mathbf{z}_\omega^{vb}$ was perturbed in the direction $\text{Re}\{\mathbf{e}_3^{vb}\}$ with speed $\omega = 547$ rad/s $\approx \omega_3^{vb}$ for the nonlinear viscoelastic model. Figures 15 and 16 show the results of these experiments. In contrast to the linear viscoelastic model, the simulations show no exponential increase of the energy or other signs of instability. These results provide strong evidence that it is the linear viscoelastic model itself that causes the non-physical exponential increase in energy. For a large range of viscoelastic parameters, we observed blow up in the linear model, but never in the nonlinear model. For the same range of parameters we also always observed that the real part of the λ_i^{vq} increases nearly linearly with the rotational speed (see Fig. 12), which suggests that no matter what parameters we choose, the $\mathbf{e}_i^{vq}$ become unstable at high enough rotational speeds. In contrast, if we look closely at the λ_i^{vb}, we see that their real parts decrease as ω increases, suggesting that the $\mathbf{e}_i^{vb}$ always remain stable; see Fig. 17.

The instability of the linear viscoelastic model is perhaps not surprising considering that the evolution operator is linear in the viscoelastic variables but is applied in a finite deformation setting. It is expected to work well for small deformations, but not so when large deformations cause nonlinear effects to become important. This is exactly what we observe: at small rotation speeds, when there is less deformation, the linear viscoelastic model
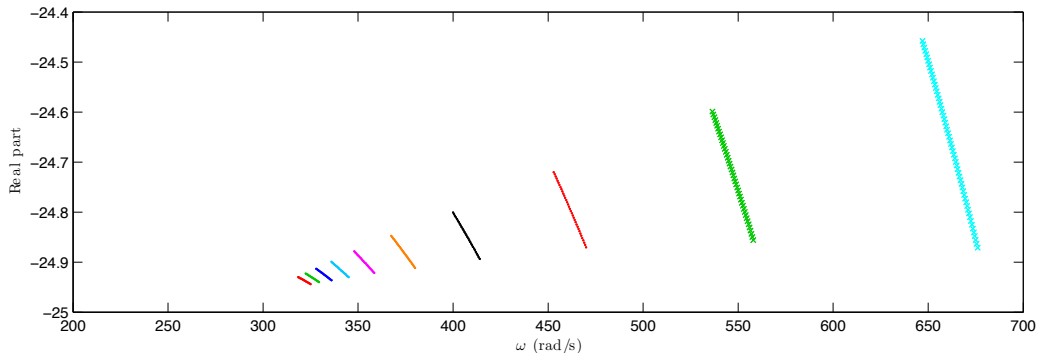
Figure 17: Plot of the real components of the λ_i^{vb}.

behaves as one expects, i.e. in a dissipative manner. However, at high speeds and large deformations the linear viscoelastic model behaves non-physically. The nonlinear viscoelastic model does not suffer from these problems since it naturally takes into account large deformations.

7. Conclusions

We have presented a formulation of the axisymmetric spinning body suitable for both steady as well as transient behavior. In the hyperelastic steady setting, we have elucidated a more complex hierarchy of bifurcation modes than have been discussed in the literature to date. This was achieved by a careful examination of the smallest magnitude eigenvalues of the linearized evolution operator. This same formulation was also extended to the finite deformation viscoelastic setting. In this setting we have identified pseudo-bifurcation modes that can be associated to a discrete set of critical frequencies. By perturbing the system from an axisymmetric state in the direction of a linearly unstable pseudo-bifurcation mode and then following the system in time, we have been able to show that the Simo-class of models for (linear) finite viscoelasticity lead to exponential growth in elastic energy in time. Thus such models are seen to be unstable, counter to intuition about convolution type models with fading memory. On the other hand, a similar analysis using a (purely) hyperelastic model is fully stable, as is a similar analysis using a Sidoroff-class model, which is necessarily thermodynamically stable. This points to the general conclusion that it is not prudent to utilize linear finite viscoelastic models of the Simo-class. In particular, in tire analyses in which a steady spinning state is perturbed to obtain a transient evolution,

26

non-physical unstable computations are clearly possible. This undesirable situation can be rectified by using nonlinear finite viscoelastic models that provably satisfy the second law of thermodynamics.

[1] J.M. Ball, *Convexity conditions and existence theorems in nonlinear elasticity*, Archives for Rational Mechanics and Analysis **63** (1977), 337–403.

[2] J.M. Bass, *Three-dimensional finite deformation, rolling contact of a hyperelastic cylinder: Formulation of the and computational results*, Computers and Structures **26** (1987), 991–1004.

[3] B. Bernstein, E.A. Kearsley, and L.J. Zapas, *A study of stress relaxation with finite strains*, Transactions of the Society of Rheology (1963), 391–410.

[4] A. Chatterjee, J.P. Cusumano, and J.D. Zolock, *On contact-induced standing waves in rotating tires: Experiment and theory*, Journal of Sound and Vibration **227** (1999), 1049–1081.

[5] P.G. Ciarlet, *Mathematical elasticity*, North-Holland, 1988.

[6] B.D. Coleman, *On thermodynamics, strain impulses, and viscoelasticity*, Archive for Rational Mechanics and Analysis **17** (1964), 230–254.

[7] _____, *Thermodynamics of materials with memory*, Archive for Rational Mechanics and Analysis **17** (1964), 1–46.

[8] B.D. Coleman and W. Noll, *The thermodynamics of elastic materials with heat conduction and viscosity*, Archive for Rational Mechanics and Analysis **13** (1963), 167–178.

[9] J.R. Dormand and P.J. Prince, *Practical Runge-Kutta processes*, SIAM J. Sci. and Stat. Comput. **10** (1989), 977–989.

[10] L.O. Faria, J.T. Oden, B. Yavari, W.W. Tworzydlo, J.M. Bass, and E.B. Becker, *Tire modeling by finite elements*, Tire Science and Technology **20** (1992), 33–56.

[11] S. Govindjee and P.A. Mihalic, *Viscoelastic constitutive relations for the steady spinning of a cylinder*, Tech. Report UCB/SEMM-98/02, University of California Berkeley, Department of Civil Engineering, 1998.

[12] S. Govindjee and S. Reese, *A presentation and comparison of two large deformation viscoelastic models*, ASME Journal of Engineering Materials and Technology **119** (1997), 251–255.

[13] R. Kennedy and J. Padovan, *Finite element analysis of steady and transiently moving/rolling nonlinear viscoelastic structure–II. Shell and three-dimensional simulations*, Computers and Structures **27** (1987), 249–257.

[14] Richard B Lehoucq, Danny C Sorensen, and Chao Yang, *ARPACK users' guide: Solution of large-scale eigenvalue problems with implicitly restarted arnoldi methods*, vol. 6, SIAM, 1998.

[15] P. LeTallec and C. Rahier, *Numerical models of steady rolling for nonlinear viscoelastic structures in finite deformations*, International Journal for Numerical Methods in Engineering **37** (1994), 1159–1186.

[16] Xiaoye S Li and James W Demmel, *SuperLU_DIST: A scalable distributed-memory sparse direct solver for unsymmetric linear systems*, ACM Transactions on Mathematical Software (TOMS) **29** (2003), 110–140.

[17] L. Nasdala, M. Kaliske, A. Becker, and H. Rothert, *An efficient viscoelastic formulation for steady-state rolling structures*, Computational Mechanics **22** (1998), 395–403.

[18] J.T. Oden and R. Lin, *On the general rolling contact problem for finite deformations of a viscoelastic cylinder*, Computer Methods in Applied Mechanics and Engineering **57** (1986), 297–367.

[19] J. Padovan, *Finite element analysis of steady and transiently moving/rolling nonlinear viscoelastic structure–I. Theory*, Computers and Structures **27** (1987), 249–257.

[20] J. Padovan and O. Paramodilok, *Generalized solution of time dependent traveling load problem via moving finite element scheme*, Journal of Sound and Vibration **91** (1983), 195–209.

[21] J. Padovan and O. Paramodilok, *Transient and steady state viscoelastic rolling contact*, Computers and Structures **20** (1985), 545–553.

[22] P.J. Rabier and J.T. Oden, *Bifurcation in rotating bodies*, Recherches en mathématiques appliquées, Masson, 1989.

[23] S. Reese and S. Govindjee, *Theoretical and numerical aspects in the thermo-viscoelastic material behaviour of rubber-like polymers*, Mechanics of Time-Dependent Materials **1** (1998), 357–396.

[24] ———, *A theory of finite viscoelasticity and numerical aspects*, International Journal of Solids and Structures **35** (1998), 3455–3482.

[25] F. Sidoroff, *Un modèle viscoélastique non linéaire avec configuration intermédiaire*, Journal de Mécanique **13** (1974), 679–713.

[26] J.C. Simo, *On a fully three-dimensional finite-strain viscoelastic damage model: Formulation and computational aspects*, Computer Methods in Applied Mechanics and Engineering **60** (1987), 153–173.

[27] C. Truesdell and W. Noll, *The non-linear field theories of mechanics*, Springer-Verlag, 1965.